CONF-8905188--2

SURFACE MAGNETO-OPTICAL STUDIES OF ULTRATHIN FERROMAGNETIC FILMS*

CONF-8905188--2

DE90 002199

C. Liu and S. D. Bader

Materials Science Division

Argonne National Laboratory, Argonne, Illinois 60439

INVITED manuscript submitted to the Second International Workshop on the Magnetic Properties of Low-Dimensional Systems, San Luis Potosi, Mexico, May 22-26, 1989, to be published by Springer-Verlag.

jmc

---

* Work supported by the U.S. Department of Energy, BES-Materials Sciences, under contract #W-31-109-ENG-38.

SURFACE MAGNETO-OPTICAL STUDIES OF ULTRATHIN FERROMAGNETIC FILMS*

C. Liu and S. D. Bader

Materials Science Division

Argonne National Laboratory, Argonne, Illinois 60439 USA

Invited manuscript submitted to
Second International Workshop on the Magnetic Properties of Low-Dimensional Systems; San Luis Potosi, Mexico, May 22-26, 1989.
to be published by Springer-Verlag.

MAY 1989

*Work supported by the U.S. Department of Energy, BES-Materials Sciences, under contract #W-31-109-ENG-38.

Surface Magneto-Optical Studies of Ultrathin Ferromagnetic Films

C. Liu and S. D. Bader

Materials Science Division
Argonne National Laboratory, Argonne, Illinois 60439 USA

The surface magneto-optic Kerr effect is used to study the existence of monolayer magnetism and the surface magnetic anisotropy of epitaxial films of Fe deposited on Cu(100), Ru(0001), and Pd(100). The critical behavior of Fe/Pd(100) is also characterized and found to be in agreement with 2-D Ising-model results.

1. Introduction

The surface magneto-optic Kerr effect (SMOKE) was introduced in 1985 to study ultrathin ferromagnetic films extending into the monolayer and submonolayer regime [1]. Since that time SMOKE has contributed significantly to the great advances that have taken place in the field of surface magnetism [2-4]. In the present work the most recent activities in our laboratory are surveyed involving the growth of Fe on Cu(100), Ru(0001), and Pd(100). These studies provide insights into three topics of interest: (i) the quest for monolayer magnetism; (ii) the nature of the surface magnetic anisotropy; and (iii) critical phenomenon in two-dimensional (2-D) magnetic systems. In the following we outline the experimental aspects of the SMOKE technique, the structural aspects of the systems, and the results of interest.

2. Experimental Technique

The films are grown in 10^{-11} Torr ultrahigh vacuum (UHV). *In-situ* SMOKE characterizations utilize crossed magnetic fields that are oriented in-plane and normal to the film plane, to sequentially monitor the corresponding magnetization components. The two configurations of the magnetic field are referred to as the longitudinal and polar Kerr-effect geometries, respectively. The electromagnets are located in UHV, while the optical source, analyzer, and the photodiode detector are separated fromUHV by a window. The source is a p-polarized He-Ne laser. The reflected light has its polarization rotated due to the magneto-optic interaction. The analyzer is a crystal prism polarizer that is nearly crossed with the incident polarization. Reversing the direction of the magnetization reverses the

rotation of the reflected light and changes the intensity at the detector. Sweeping the field provides magnetic hysteresis curves, whose height, referred to as the Kerr intensity, is proportional to the magnetization M. If the easy axis is in-plane along the applied-field direction the longitudinal SMOKE signal yields a square loop and the polar signal yields no hysteresis. If the easy axis is vertical the polar loop is square and the longitudinal signal is absent.

3. Structural Characterizations

3.1 Epitaxy

Low-energy electron diffraction (LEED) is used to monitor the epitaxy. The Fe films all grow epitaxially in the thickness range reported, based on the fcc or γ-Fe structure, and take on the substrate in-plane lattice spacing. The interplanar spacings are characterized by layer-dependent tetragonal distortions due to both interfacial strain and surface relaxation. The distortions are approximately -2% and +2%, respectively, for Fe/Cu(100), based on quantitative LEED studies [5]. The distortions are anticipated to be more pronounced for the Ru and Pd cases than for Cu because of the in-plane lattice mismatch. The fcc Fe(111) orientation grows on Ru(0001) with the expanded Ru intralayer spacing of 2.70 Å *vs.* 2.54 Å for the equilibrium γ-Fe value, which is obtained by extrapolation from above 910° C where bulk γ-Fe is stable. The Fe/Pd(100) structure is expected to be body centered tetragonal (bct) based on recent quantitative LEED studies for the related system Mn/Pd(100) [6]. The bct phase is derived from distortion of the fcc-Fe structure. The Pd(100) intraplanar distances are 2.75 Å. The tetragonal interplanar distortions inherent in epitaxial films have important consequences for the magnetic anisotropy because the magnetocrystalline contribution could favor vertical easy axes of magnetization [7]. This point will be discussed when the anisotropy results are presented.

3.2 Growth Mode

Auger electron spectroscopy is used to monitor the surface cleanliness and the film growth mode. The standard procedure is to measure the substrate and Fe Auger signals during growth, and then to compare them to growth-model predictions [7-8]. The general inference is that the films grow predominantly in a layer-by-layer fashion. Advanced structural techniques, such as RHEED and photoelectron diffraction, have helped to refine our growth techniques [9]. From these studies we learn that homoepitaxial growth at elevated temperatures prior to Fe deposition atomically smoothes the substrate surface, and that subsequent

low-temperature Fe deposition promotes discrete interfaces. Interfacial mixing for Fe/Cu(100) has dramatic consequences, in that it can stabilize the antiferromagnetic state of γ-Fe [10].

4. Results and Discussion

4.1 Monolayer Magnetism

Figures 1-3 summarize our magnetic characterizations of Fe on Cu, Ru, and Pd, respectively. The existence of monolayer (ML) magnetism is related to two issues: the ability to create monolayers, and the intrinsic electronic structure of the monolayer. For Fe/Cu(100) a ferromagnetic response is not detected at the monolayer level because of the tendency to intermix [2]. The problem is related to the high surface free energy of Fe relative to that of Cu. For this reason growth on Ru was initiated. However, Fig. 2 shows that monolayer levels of Fe on Ru(0001) also lack a ferromagnetic signature. We relate this to the hybridization of the Fe and Ru d-electrons across the interface. For dilute Fe impurities in a Ru host it is well known that hybridization suppresses moment formation [11]. For Fe on Pd(100) Fig. 3 shows that even submonolayer magnetism is detected. The hybridization in this case is expected not only to preserve the Fe moment, but also to induce moments on neighboring Pd sites. Recall that dilute alloys of Fe in Pd hosts are classic giant-moment systems [12]. Thus, the interactions with the substrate can yield compositional gradients and/or electronic structural modifications that govern the magnetic state of the film.

4.2 Surface Magnetic Anisotropy

Figures 1-3 also summarize the anisotropy results. For Fe/Cu(100) the region of perpendicular spin orientations is delineated as a function of growth temperature and film thickness. The Ru and Pd results are at fixed growth-temperatures. Note that in all three cases there exists a critical thickness above which the easy axis reorients in-plane. This provides a clue that the perpendicular anisotropy originates more from the surface and interfacial properties than from the geometric distortions discussed above that should persist throughout the thickness range.

The anisotropy diagrams of Figs. 1-3 are for measurement at the growth temperature. The vertical state, however, can be retained above the high-temperature boundaries by raising temperature subsequent to growth. The 1.2-ML Fe/Pd(100) film grown at ~100K could be taken above the 270-K boundary (not shown in Fig. 3) and up to the Curie temperature T_C without reorienting.

4.3 Critical Behavior

Dürr, *et al* [13] recently extracted the critical magnetization exponent β_C for Fe/Au(100), and reviewed previous work in the field. There are numerous motivations to pursue the issue further. Firstly, we have found that Fe/Pd(100) has an advantage of thermal stability and reversibility, while Fe/Au(100) can be susceptible to segregation and intermixing problems [8]. Secondly, Fe/Pd(100) has the additional advantage of permitting studies of vertical as well as in-plane spin orientations, while the magnetization of Fe/Au(100) is only in-plane. Finally, the β-value of 0.22±0.05 reported for Fe/Au(100) disagrees with the expected 2-D Ising $\beta_C=1/8=0.125$. An Ising-model exponent is expected even though the films are physical realizations of Heisenberg systems [14] because even arbitrarily small anistropy causes the 2-D Heisenberg system to yield an Ising-like transition.

Figure 4 shows the M-*vs.*-T curves for different film thicknesses and spin orientations, including warming and cooling data to illustrate the high degree of reversibility of the transitions. M represents the normalized Kerr intensity measured in the remanent state (H=0) for films that exhibit square-loop hysteresis curves. Thus, no external fields are present to add tails that extend the transitions to higher temperatures. However, significant tails are present, presumably due to the interactions with the highly polarizable interfacial Pd. Dürr, *et al* [13] outlined methodology for extracting β in the presence of high-temperature tailing superimposed on the power-law behavior. We follow their procedure and parametrize T_C to extend the range of linearity of the traditional log-log plots used to extract β, where $M\propto(1-T/T_C)^{\beta}$. The results are shown in Fig. 5 and the T_C-values are plotted in Fig. 6. The 1.2-ML film has the densest data set, and, therefore, was subjected to the most thorough analysis, which yields $\beta=0.127\pm0.004$. Thus, agreement with the 2-D Ising result of $\beta=0.125$ is achieved.

The trend in the T_C-values in Fig. 6 is compared with that obtained from Monte Carlo calculations of Binder and Hohenberg [15] for 2-D Ising models. Their results for integral layer thicknesses, normalized to experiment at 3 ML, are shown connected by the dashed curve. There is quite good agreement between experiment and calculation. Recent theoretical work by Bander and Mills [14] predicted that T_C would decrease in the vicinity of the critical thickness value for vertical easy axes, based on a 2-D Heisenberg model with spin-orbit-only anisotropy. The monotonic increase of the experimental T_C-values, however, is contrary to their prediction and suggests that multiple anisotropies are at play.

5. Summary

Three issues in surface magnetism are addressed using SMOKE characterizations of the magnetic properties of the epitaxial systems Fe on

Cu(100), Ru(0001), and Pd(100). The first issue concerns the criteria for and impediments to achieving monolayer magnetism. The second involves the nature and origin of the surface magnetic anisotropy. Both of these issues involve the competing influence of electronic and geometric structural considerations. The last issue of the critical behavior involves the dimensionality more straightforwardly. Taken together the three illustrate the richness of opportunities and challenges in the field of low-dimensional magnetism.

Acknowledgement

This work was supported by the U. S. Department of Energy, Basic Energy Sciences-Material Sciences, under Contract W-31-109-ENG-38.

6. References

1. E. R. Moog and S. D. Bader, Superlattices Microstruct. 1, 543 (1985); S. D. Bader, E. R. Moog, and P. Grünberg, in *Magnetic Properties of Low Dimensional Systems*, Springer Proceedings in Physics 14, edited by L. M. Falicov and J.-L. Mòran- Lôpez (Springer-Verlag, Berlin, 1986) p. 70.
2. C. Liu, E. R. Moog, and S. D. Bader, Phys. Rev. Lett. 60 2422 (1988).
3. T. Beier, H. Jahrreiss, D. Pescia, Th. Woike, and W. Gudat, Phys. Rev. Lett. 61 1875 (1988).
4. J. Araya-Pochet, C. A. Ballentine, and J. L. Erskine, Phys. Rev. B 38, 7846 (1988).
5. S. H. Lu, J. Quinn, D. Tian, F. Jona, and P. M. Marcus, preprint.
6. D. Tian, S. C. Wu, F. Jona and P. M. Marcus, Solid State Commun. (1989) in press.
7. M. Stampanoni, A. Vaterlaus, M. Aeschlimann, F. Meier, and D. Pescia, J. Appl. Phys. 64 5321, (1988) .
8. S. D. Bader and E. R. Moog, J. Appl. Phys. 61, 3729 (1987).
9. W. F. Egelhoff, Jr., and I. Jacob, Phys. Rev. Lett. 62 921 (1989).
10. W. A. A. Macedo and W. Keune, Phys. Rev. Lett. 61 475, (1988).
11. A. M. Clogston, B. T. Matthias, M. Peter, H. J. Williams, E. Corenzwit, and R. C. Sherwood, Phys. Rev. 125, 541 (1962).
12. J. Crangle, Phil Mag. 5 335 (1960).
13. W. Dürr, M. Taborelli, O. Paul, R. Germar, W. Gudat, D. Pescia, and M. Landolt, Phys. Rev. Lett. 62, 206 (1989).
14. M. Bander and D. L. Mills, Phys. Rev. B 38 12015 (1988).
15. K. Binder and P. C. Hohenberg, IEEE Trans. on Magnetics, MAG-12 66 (1976).

Figure Captions

Figure 1. Anisotropy diagram for Fe/Cu(100). Note the region of stability of perpendicular easy axes with square hysteresis loops in the polar SMOKE signal.

Figure 2. Anisotropy diagram of Fe/Ru(0001) grown at room temperature plotted as the height of the hysteresis curve in the remanent state. Note the critical thickness where the magnetization reorients in-plane; the longitudinal SMOKE signals become finite and the polar signal vanishes. Note also the lack of ferromagnetic signature at the monolayer level based on null measurements and dashed-line extrapolations.

Figure 3. Anisotropy diagrams for Fe/Pd(100) for (a) 300-K and (b) 100-K growth. Note the critical thickness transition in (b), and the existence of submonolayer magnetism.

Figure 4. Normalized M-*vs.*-T curves for Fe/Pd(100). The top panel is for in-plane easy axes (300-K growth), and the bottom panel is for vertical easy axes (100-K growth).

Figure 5. Log-log plots for Fe/Pd(100). The fitted β-values compare favorably with the 2-D Ising value of $\beta_C=1/8=0.125$.

Figure 6. T_C *vs.* thickness for Fe/Pd(100). The dashed line connects the 2-D Ising-model results of Binder and Hohenberg for integral layer thicknesses, normalized to experiment at 3 ML.

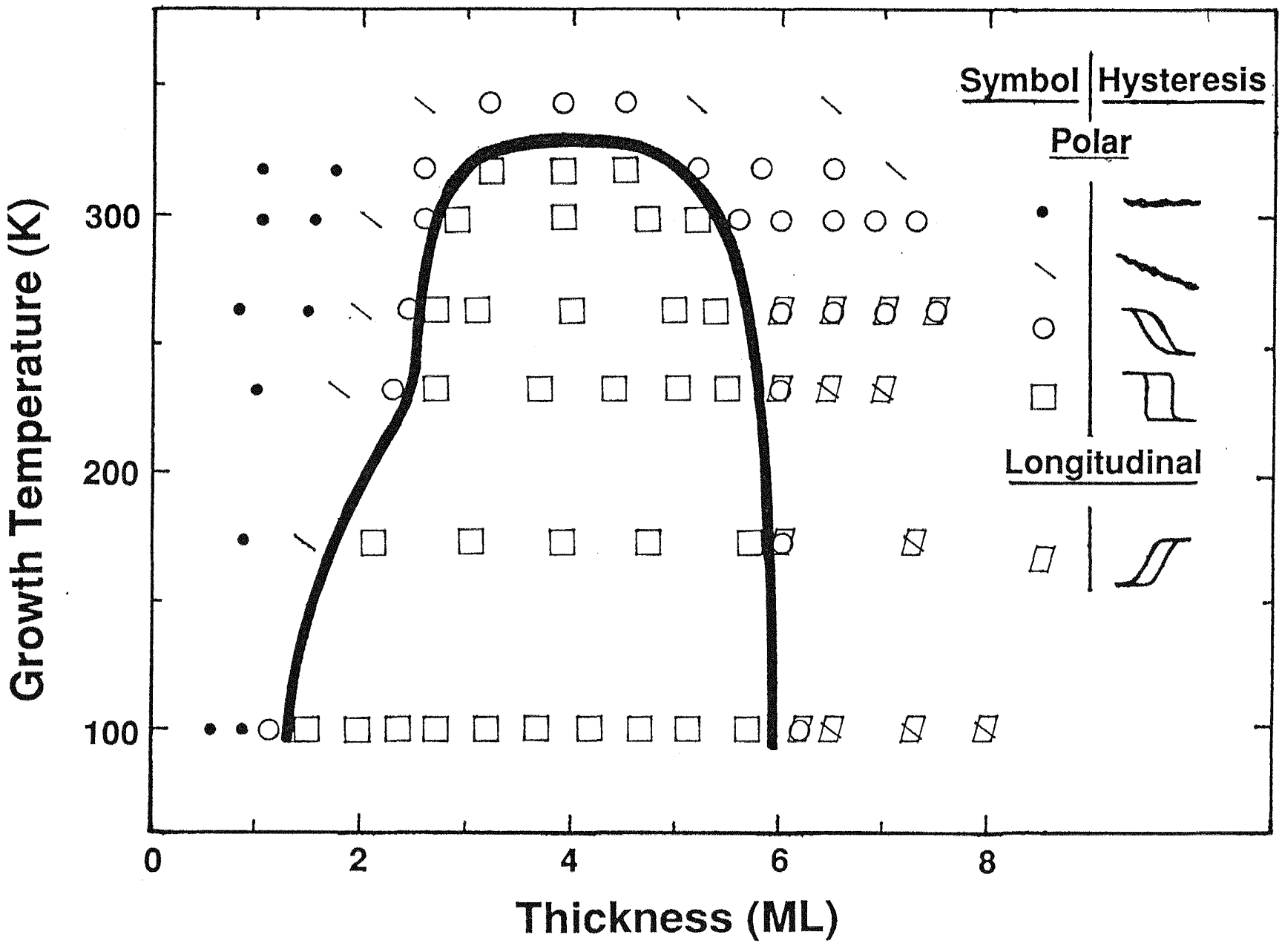

— C. Liu and S. D. Bader FIG. 1 —

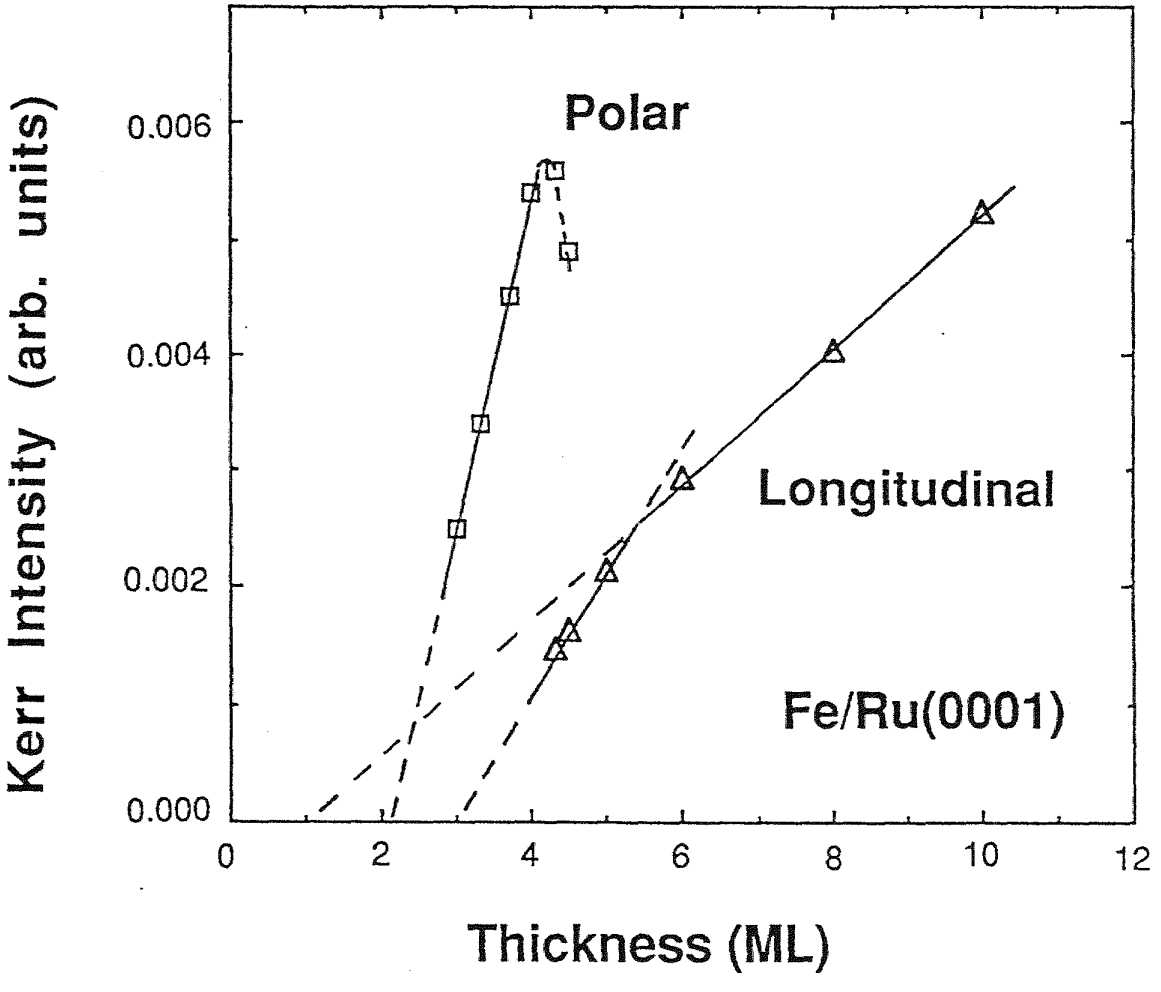

— C. Liu and S.D. Bader Fig. 1 —

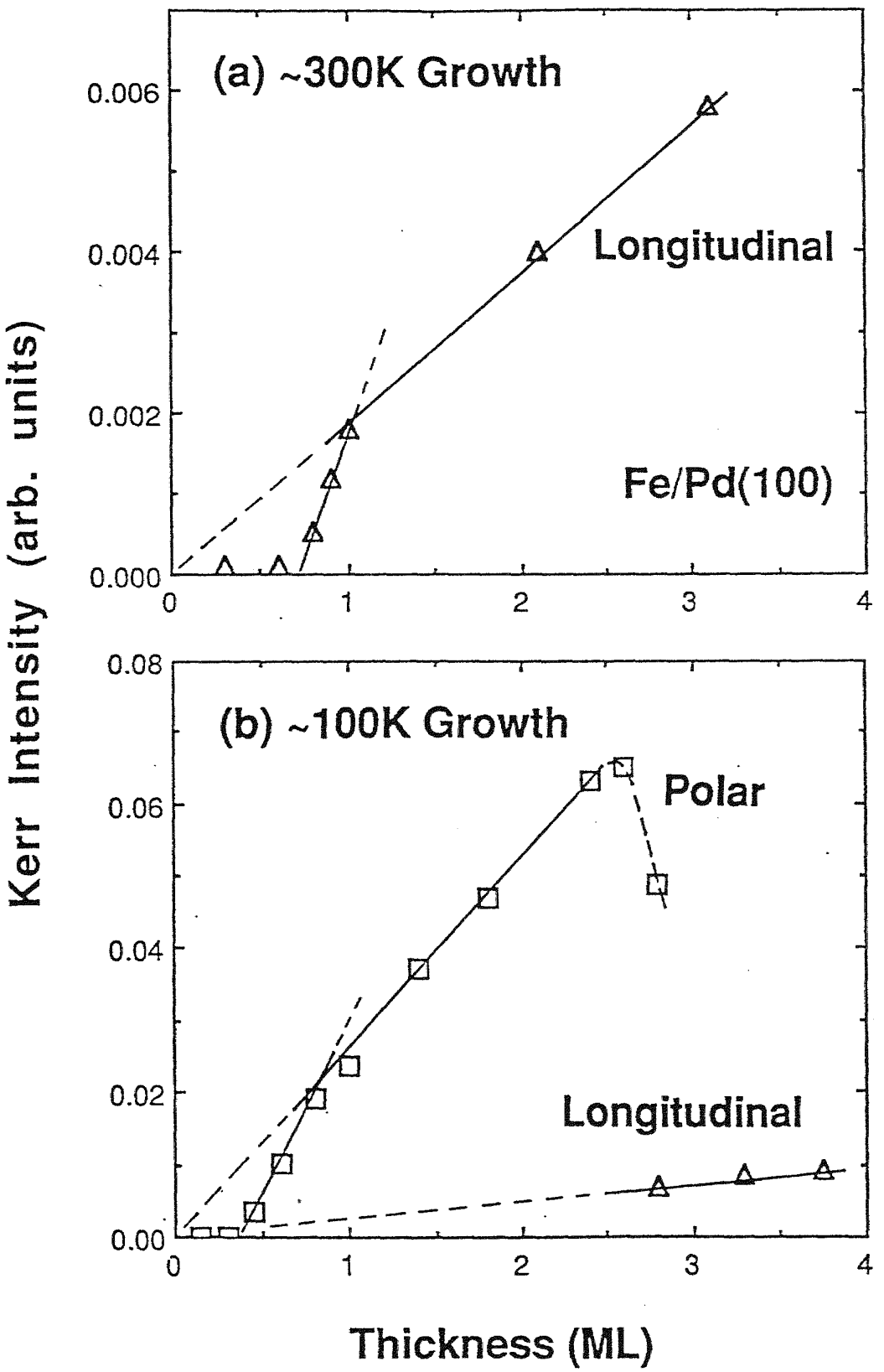
(a) ~300K Growth
Longitudinal
Fe/Pd(100)
0.006
0.004
0.002
0.000
0
1
2
3
4
(b) ~100K Growth
Polar
Longitudinal
0.08
0.06
0.04
0.02
0.00
Kerr Intensity (arb. units)
Thickness (ML)

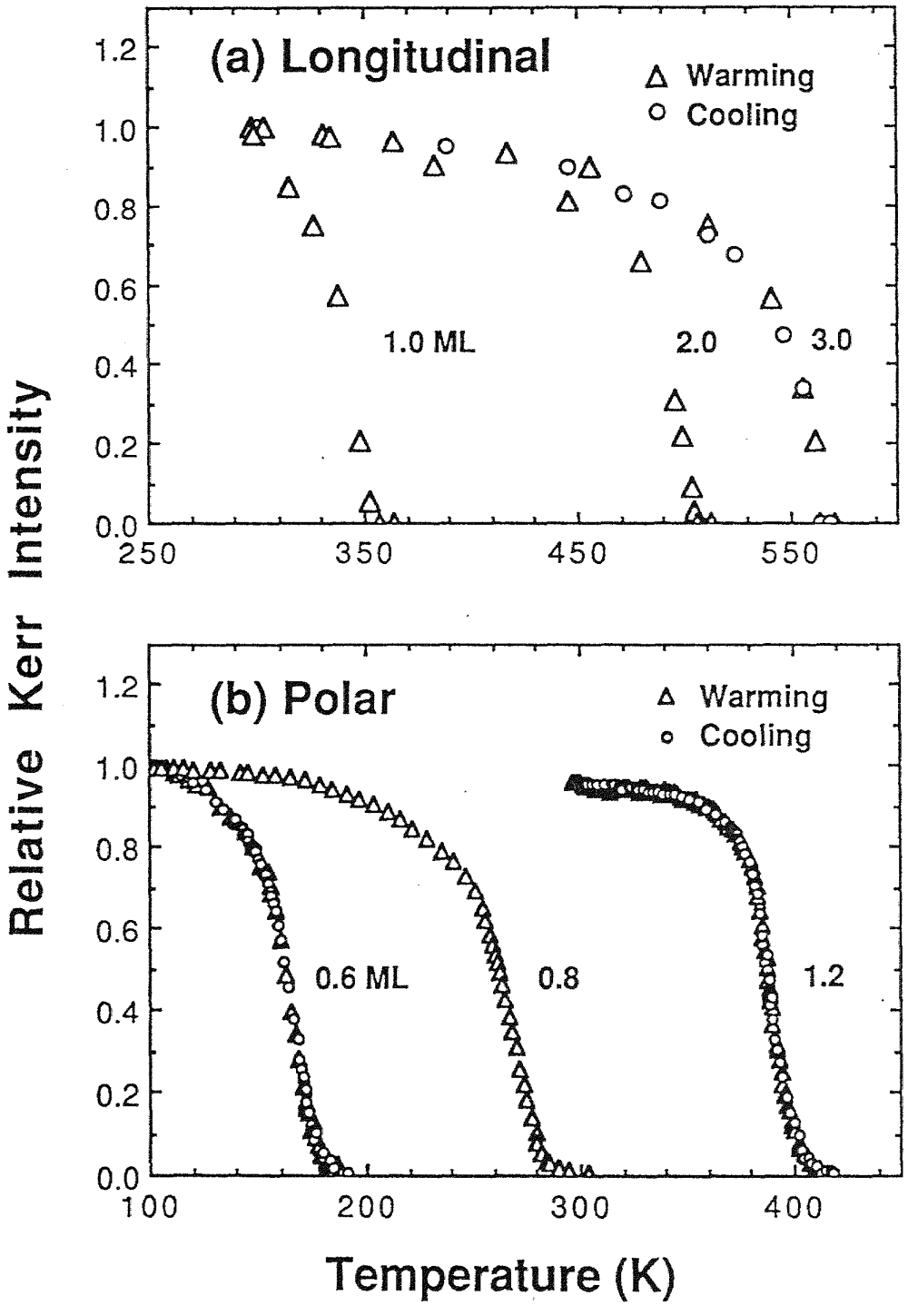
(a) Longitudinal
Warming
Cooling
1.0 ML
2.0
3.0
(b) Polar
Warming
Cooling
0.6 ML
0.8
1.2
Relative Kerr Intensity
Temperature (K)
0.0
0.2
0.4
0.6
0.8
1.0
1.2
250
350
450
550
100
200
300
400

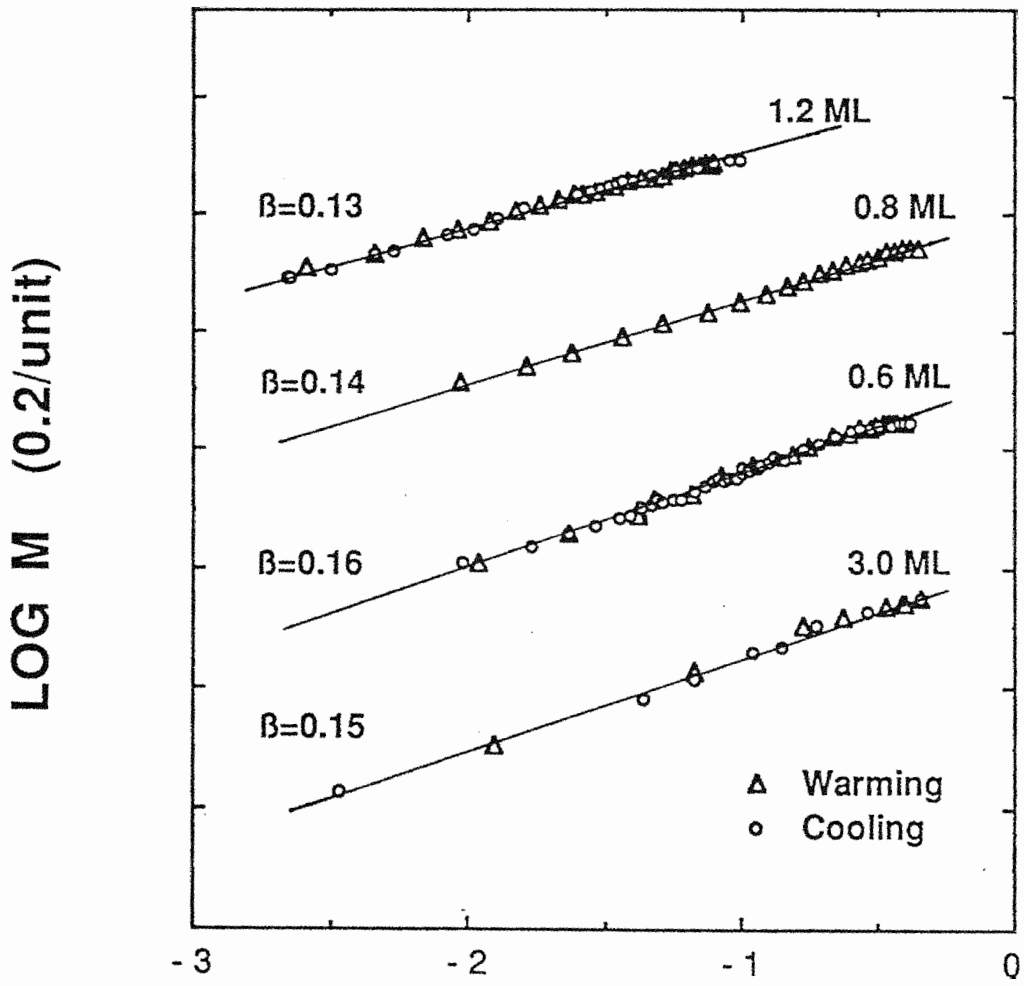
1.2 ML
ß=0.13
0.8 ML
ß=0.14
0.6 ML
ß=0.16
3.0 ML
ß=0.15
Warming
Cooling
- 3
- 2
- 1
0
LOG M (0.2/unit)
LOG(1-T/Tc)

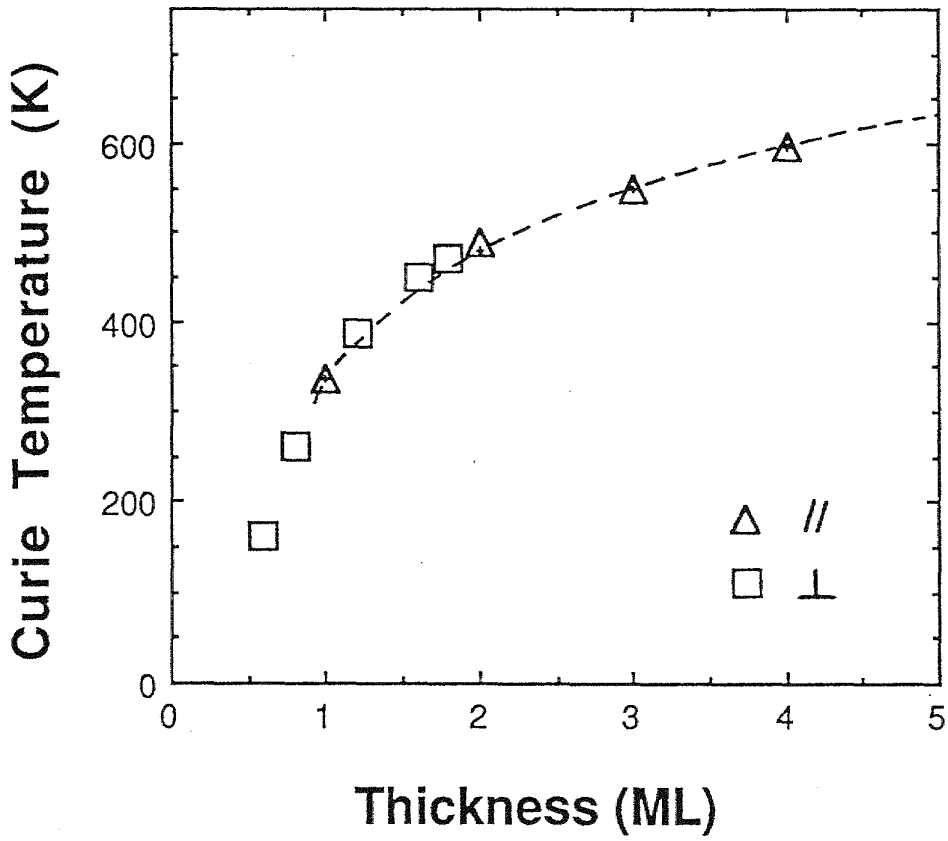

— S. D. Bader Fig. 6 —